

# CHEM MED CHEM

CHEMISTRY ENABLING DRUG DISCOVERY

## Accepted Article

**Title:** Phenyl boronic acids development led to validated leads active in clinical strains overexpressing KPC-2: a step against bacterial resistance.

**Authors:** Giuseppe Celenza, Mattia Vicario, Pierangelo Bellio, Linciano Pasquale, Mariagrazia Perilli, Antonio Oliver, Jesus Blazquez, Laura Cendron, and Donatella Tondi

This manuscript has been accepted after peer review and appears as an Accepted Article online prior to editing, proofing, and formal publication of the final Version of Record (VoR). This work is currently citable by using the Digital Object Identifier (DOI) given below. The VoR will be published online in Early View as soon as possible and may be different to this Accepted Article as a result of editing. Readers should obtain the VoR from the journal website shown below when it is published to ensure accuracy of information. The authors are responsible for the content of this Accepted Article.

**To be cited as:** *ChemMedChem* 10.1002/cmdc.201700788

**Link to VoR:** <http://dx.doi.org/10.1002/cmdc.201700788>

WILEY-VCH

[www.chemmedchem.org](http://www.chemmedchem.org)

A Journal of



# “Phenyl boronic acids development led to validated leads active in clinical strains overexpressing KPC-2: a step against bacterial resistance”

Giuseppe Celenza<sup>[a]</sup>, Mattia Vicario<sup>[b]</sup>, Pierangelo Bellio<sup>[a]</sup>, Pasquale Linciano<sup>[c]</sup>,  
Mariagrazia Perilli<sup>[a]</sup>, Antonio Oliver<sup>[d]</sup>, Jesús Blazquez<sup>[e]</sup>, Laura Cendron<sup>[b]\*</sup> and Donatella Tondi<sup>[c]\*</sup>

- [a] Dr. G. Celenza, <https://orcid.org/0000-0003-2796-9228>, Dr. P. Bellio, Prof. M. Perilli  
Dipartimento di Scienze Cliniche Applicate e Biotecnologie.  
Università dell'Aquila,  
Via Vetoio, 1, 67100 L'Aquila, Italy
- [b] Dr. M. Vicario, Dr. L. Cendron, <https://orcid.org/0000-0002-0125-0461>, **E-mail:** [laura.cendron@unipd.it](mailto:laura.cendron@unipd.it)  
Dipartimento di Biologia, Department  
Università di Padova,  
Viale G. Colombo 3, 35121, Padova, Italy
- [c] Dr. P. Linciano, Dr. D. Tondi, <https://orcid.org/0000-0002-5195-5531>, **E-mail:** [tondid@unimore.it](mailto:tondid@unimore.it)  
Dipartimento di Scienze della Vita,  
Università di Modena e Reggio Emilia,  
Via Campi 103, 41100, Modena, Italy.
- [d] Dr. A. Oliver  
Servicio de Microbiología and Unidad de Investigación.  
Hospital Universitario Son Espases, Instituto de Investigación Sanitaria de Mallorca,  
Palma de Mallorca, Spain
- [e] Dr. J. Blazquez  
Department of Microbial Biotechnology, National Center for Biotechnology,  
Consejo Superior de Investigaciones Científicas (CSIC),  
C/ Darwin, 3, Campus de la Universidad Autonoma-Cantoblanco, 28049-Madrid, Spain

Supporting information for this article is given via a link at the end of the document.

**Abstract:** The emergence and dissemination of multi drug resistant (MDR) pathogens resistant to near all available antibiotics poses a significant threat in clinical therapy. Among them, *Klebsiella pneumoniae* clinical isolates overexpressing KPC-2 carbapenemase are the most worrisome, extending bacterial resistance to last resort carbapenems. In this study we investigate the molecular recognition requirements in KPC-2 active site by small phenyl boronic acid derivatives. Four new phenyl boronic acid derivatives were designed and tested vs KPC-2. For the most active, despite their simple chemical structures, nanomolar affinity was achieved. New derivatives restored susceptibility to meropenem in clinical strains overexpressing KPC-2. Moreover no cytotoxicity was detected in cell viability assays, further validating the designed leads. Two crystallographic binary complexes of best inhibitors binding KPC-2 were obtained at high resolution. Kinetic descriptions of slow binding, time dependent inhibition and interactions geometries in KPC-2 were fully investigated. This study will ultimately lead toward optimization and development of more effective KPC-2 inhibitors.

## Introduction

The emergence of bacterial strains resistant to available antibiotic armamentarium is nowadays a pressing issue in clinical therapy. Among the several mechanisms of bacterial

resistance, the rapid evolution and spread of carbapenemases,  $\beta$ -lactamases (BLs) with versatile hydrolytic capacities able to inactivate last resort carbapenems, represents a menace in treating highly resistant infections.<sup>[1-7]</sup>

Carbapenem-resistant Enterobacteriaceae (CREs), reported with increased frequency, are progressively spreading throughout the world thus leaving no effective antibiotics.<sup>[1,2,5,6,8]</sup> In particular CREs possessing *bla*KPC-2 (e.g. *Klebsiella pneumoniae*) are high-priority target pathogens for the development of novel antibacterials: KPC-producing organisms confer resistance not only to all available  $\beta$ -lactams antibiotics (including aminothiazoleoxime cephalosporins such as cefotaxime) but also to other antimicrobial classes such as fluoroquinolones and aminoglycosides.<sup>[9-11]</sup> Moreover KPCs are weakly inhibited by therapeutically available  $\beta$ -lactamase inhibitors (i.e. clavulanic acid, Figure 1a).<sup>[12]</sup> As a consequence, KPCs mediated infections are difficult to treat and often associated with high therapeutic failure and high mortality rates, making KPCs a major global health threat.<sup>[13,14]</sup>

Among developed carbapenemases inhibitors, novel chemical entities not resembling the  $\beta$ -lactam ring are rare, with few exceptions such as the recent approved avibactam (Figure 1b).<sup>[15]</sup> This non  $\beta$ -lactam (BL) inhibitor, able to restore susceptibility to  $\beta$ -lactams when administered in combination, is however slowly hydrolyzed by KPC-2, suggesting peculiarities in the catalytic mechanism for class A carbapenemase.<sup>[15]</sup>

In the *de novo* BL inhibitors scenario, boronic acid derivatives play an interesting role: they possess a non  $\beta$ -lactam moiety and act as competitive inhibitors of BLs, covalently, but reversibly, binding the catalytic serine of BLs belonging to class A, C and D.<sup>[16–21]</sup> Very recently boronic acids have also been reported to inhibit zinc-dependent BLs, opening the way for the development of dual action inhibitors.<sup>[22–23]</sup> RPX7009, a highly potent inhibitor of KPC is currently in development.<sup>[24]</sup>

At present few crystal structures of KPC-2 in its apo and complexed form have been disclosed making KPC-2 an attractive target for structure based drug design: there is still much to be done to fully understand KPC-2 catalysis machinery and its ability to overcome carbapenems action.<sup>[2]</sup>

We report here the rational optimization of phenyl boronic acid derivatives acting as novel, non  $\beta$ -lactam like inhibitors *via* a time dependent mechanism of inhibition (Figure 1c). For the two most active compounds, X-ray crystallographic binary complexes were determined, confirming that designed molecules take advantage of critical consensus binding sites, peculiar of KPC-2 and other class A carbapenemases. The best inhibitor, in light of its nanomolar affinity for the enzyme, its ligand efficiency of 0.62 kcal mol<sup>-1</sup>, its ability to synergize in clinical isolates last resort carbapenem meropenem and its no-cytotoxicity, was validated as lead-like molecule.<sup>[25]</sup>

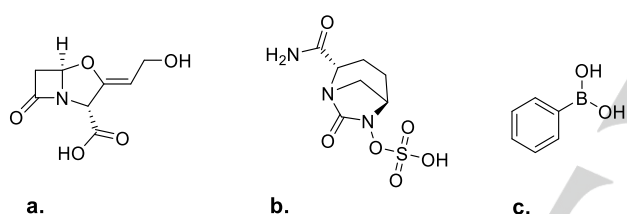


**Figure 1.** Clavulanic acid, a  $\beta$ -lactam base inhibitor (a); Avibactam, a KPC-2 *de novo* inhibitor (b); phenyl boronic acid (c)

## Results and Discussion

### Design and synthesis

Starting from **1** (Table 1), a micromolar inhibitor of KPC-2 ( $K_i$  7.64  $\mu$ M) with detectable synergic activity towards organisms overexpressing KPC-2, we were interested in obtaining a validated lead with improved affinity to KPC-2 carbapenemase and most importantly able to significantly restore susceptibility to carbapenems in pathogen overexpressing KPC-2 (Table 1). Taking into account specific binding requirements in KPC-2, to localize the most appropriate point of derivatization in **1** and to rationally select proficuous chemical groups suitable for derivatization, we referred to available X-ray structures of KPC-2, binding respectively the 3-nitro-phenyl boronic, a close analogue of compound **1**, and the antibiotic avibactam (Figure 1b).<sup>[15,26]</sup>

In a possible derivatization of phenyl boronic acid **1**, we reasoned that the introduction of a carboxylic group mimicking the C3(4') carboxylate of  $\beta$ -lactam antibiotics, a key recognition feature in BLs, might improve KPC-2 binding via a large interaction network with Arg-220, Ser-130, Thr-237 and Thr-235. All mentioned residues are located in the  $\beta$ -lactam carboxylate-binding pocket where the sulfate group of avibactam, as well as the carboxylic group of other known class A inhibitors, are known to bind.<sup>[17,27]</sup>

While the presence of the boronic acid group guarantees a covalent linking to Ser-70, sinking *de facto* the inhibitor in the active site, a proper linker could correctly orient the lateral carboxylic chain in the targeted site, without preventing other classical interactions between the ligand and residues Thr-237, Glu-166 and Asn-170, as seen in the KPC-2-3-nitro-phenyl boronic complex.<sup>[26]</sup>

With the purpose of mimicking distance, chemistry, and interactions of C3(4') carboxylate of  $\beta$ -lactam antibiotics, structural considerations suggested to introduce a carboxylic moiety, properly spaced by a two atomic vinyl chain, in the *ortho* position, adjacently to boronic group of compound **1**. Therefore, compound [2-(2-carboxyvinyl)phenyl]boronic acid (**2**) was selected as a promising compound **1** candidate derivative (Table 1). Moreover its ethyl derivatives [2-(2-carboxyethyl)phenyl]boronic acid (**4**) was synthesized *ad hoc* to introduce flexibility on the lateral chain of **2** with the aim to evaluate its contribution in overall binding and optimal rearrangement. For both derivatives the corresponding analogues, carrying the lateral carboxylic chain in *meta* (**3** and **5**) were selected as non-proficuous probes and evaluated for their affinity to KPC-2. Compounds **3** and **5**, carrying a non-optimally oriented lateral chain, could support the validation of **2** and **4** while investigating enzyme plasticity.

**Table 1.** Phenyl boronic acid **1** and its optimized derivatives: improving binding affinity vs KPC-2.

Code	Structure	$IC_{50}$ ( $\mu$ M) <sup>[a]</sup>	$K_i$ ( $\mu$ M)
<b>1</b>		31.9	7.64 <sup>[b]</sup>
<b>2</b>		10.1	2.43 <sup>[c]</sup>
<b>3</b>		130.1	31.17 <sup>[b]</sup>
<b>4</b>		4.72	1.13 <sup>[c]</sup>
<b>5</b>		221.3	53.02 <sup>[b]</sup>

<sup>[a]</sup> Determined vs KPC-2 (3.1 nM), Phosphate buffer 50 mM, pH 7.0, reporter substrate nitrocefim. <sup>[b]</sup> Estimated from  $IC_{50}$  as per competitive inhibitor from Cheng-Prusoff equation. Reporter substrate Nitrocefim at 115  $\mu$ M. <sup>[c]</sup> Estimated from  $IC_{50}$  as per competitive inhibitor from Cheng-Prusoff equation. Reporter substrate Nitrocefim at 300  $\mu$ M. All the experiments were performed in triplicate. Experimental error never exceeds 5%.

### BL Inhibition Studies and Susceptibility Assays.

In order to investigate the inhibitory activity of the phenyl boronic acid derivatives, KPC-2 full-length and KPC-2 C-terminus deletion were overexpressed and purified in a single chromatographic step, yielding more than 150 mg of protein per liter of culture, with a purity degree higher than 99%. In our experimental conditions, the  $K_M$  for nitrocefim measured for KPC-2 full-length has been determined as 36.0  $\mu$ M.<sup>[26,28,29]</sup>

$K_i$  values for derivatives **1-5** were obtained from  $IC_{50}$  as per competitive inhibition (Cheng-Prusoff equation), in agreement with the inhibition patterns in this series of compounds and with

experiments investigating the effect of increasing substrate concentrations (Table 1).

Binding reversibility was determined, for all derivatives, by measuring the recovery of the enzymatic activity after a rapid and large dilution of the enzyme-inhibitor complex. While **1**, **3** and **5** behave as rapid fully-reversible inhibitors, **2** and **4** exhibit slow reversibility, as observed from the peculiar shape of the time-course curve (Figure 2).<sup>[30]</sup>

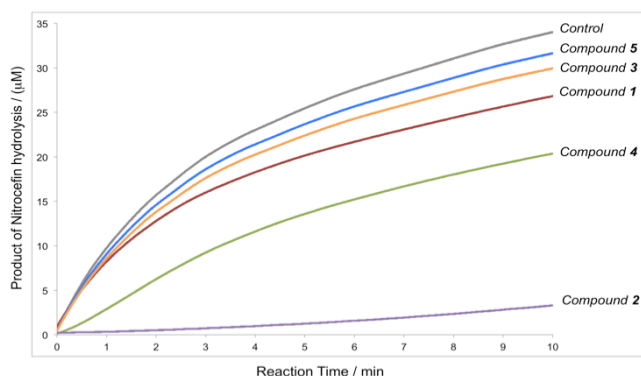


**Figure 2.** Recovery of KPC-2 activity after rapid dilution of the enzyme-inhibitor complex. The curve in gray refers to the control sample pre-incubated and diluted in the absence of inhibitor. Curves in magenta, orange and blue refer to **1**, **3** and **5** respectively at 40  $\mu\text{M}$ , 150  $\mu\text{M}$  and 250  $\mu\text{M}$ . These compounds behave as rapidly reversible inhibitors. The curve in green describes the time-course of the slowly reversible compound **4** at 12  $\mu\text{M}$ . Specifically the slow reversibility is visible in the first 2 minutes where the shape of the curve is indicative of a measurable recovery of enzymatic activity. The curve in purple is the time-course of compound **2** at 6  $\mu\text{M}$ , acting as a very slowly reversible inhibitor.

For **2** and **4**, behaving as slowly reversible inhibitors, the apparent and true constants of inhibition were therefore determined, as well as the rate constants of the isomerization steps ( $k_{+2}$  and  $k_{-2}$ ) (Figure 3A-D, Table 2).<sup>[31,32]</sup>

As usual for this mechanism of inhibition, the  $k_{+2}$  rate constant resulted higher than the  $k_{-2}$  rate constant for both analyzed compounds.

The high affinity inhibition constants  $K_i^*$  for **2** and **4** are respectively 6-fold and 8-fold lower than those calculated for the initial encounter complex (Table 2).

Both compounds behave as competitive inhibitors as demonstrated by the hyperbolic decrease of the  $k_{obs}$  value at increasing reporter substrate concentrations (Figure 4A and 4B). Affinity data for designed *ortho* derivatives **2** and **4** show, as expected, a potency improvement vs KPC-2 (3-7 fold, considering the initial encounter complex) with respect to **1**, while the derivatization in *meta* in **3** and **5** was detrimental (4 and 7-fold loss in activity respectively). The *meta* substitution in fact does not allow an optimal orientation of the lateral carboxylated chain and reasonably affect negatively phenyl boronic overall binding orientation. They served as non-proticuous ligands highlighting the importance of correctly predicting and orienting new binding interactions without perturbing preexistent binding geometry (Table 1).

When comparing binding affinity for compounds **2** and **4**, acting as slowly reversible inhibitors, however, the true constants of inhibition  $K_i^*$  must be considered. As a consequence the improvement of potency for **2** and **4** largely exceeded one order of magnitude with respect to **1** (0.43  $\mu\text{M}$  and 0.14  $\mu\text{M}$  for **2** and **4**

respect to 7.64  $\mu\text{M}$  of **1**, 18 and 55 fold improvement respectively) thus corresponding to an increase of at least 2.65 Kcal/mol, coherent with the designed additional H-bond interaction ( $\Delta\Delta G = RT \ln(K_{i \text{ compound } 2} / K_{i \text{ compound } 1})$ ).

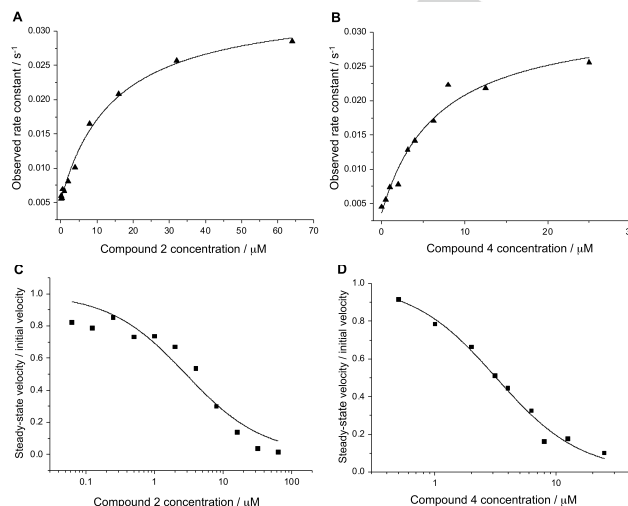


**Figure 3.** Kinetics characterization of (A) **2** and (B) **4**. Plots of  $k_{obs}$  as a function of the slow binding inhibitor conforming to the two-step mechanism (equation A.2, see methods). Experimental data fitted to equation A.3 shows a hyperbolic function of inhibitor concentration [I]. The intercept of the curve on the y-axis can be used to estimate the  $k_{-2}$  value, while the horizontal asymptote at infinite inhibitor concentration (maximum value of  $k_{obs}$ ) represents the sum of  $k_{+2}$  and  $k_{-2}$  values. Concentration-response plots for the final inhibited states of (C) **2** and (D) **4**.  $K_i^{app}$  can be calculated as the half-maximal concentration of the isotherm of the fractional velocity  $v_{ss}/v_0$  (where  $v_0$  is the initial rate of the uninhibited reaction) as a function of the decimal logarithm of the inhibitor concentrations. All the experiments were performed in triplicate. Experimental error never exceeds 5%.

**Table 2.** Compounds **2** and **4** time dependent, slow reversible kinetics parameters.

#	$k_{max}$ ( $s^{-1}$ )	$k_{-2}$ ( $s^{-1}$ )	$k_{+2}$ ( $s^{-1}$ )	$K_i^{app}$ ( $\mu\text{M}$ )	$K_i^*$ ( $\mu\text{M}$ )	$K_i^{app}$ ( $\mu\text{M}$ )	$K_i^*$ ( $\mu\text{M}$ )
<b>2</b>	$2.92 \times 10^{-2}$	$2.40 \times 10^{-2}$	$5.22 \times 10^{-3}$	2.86	0.43	14.57	2.43
<b>4</b>	$2.89 \times 10^{-2}$	$2.53 \times 10^{-2}$	$3.59 \times 10^{-3}$	3.2	0.14	6.79	1.13

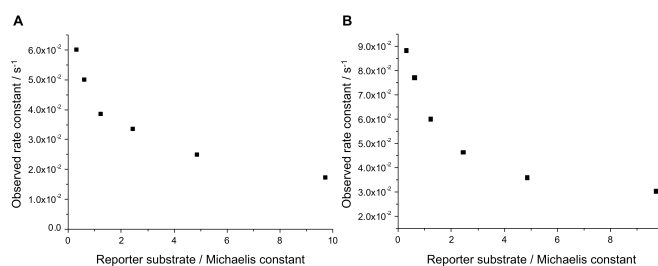


**Figure 4.** Effect of reporter substrate concentration (relative to  $K_M$ ) on  $k_{obs}$  for **2** at 12  $\mu\text{M}$  (A) and **4** at 6  $\mu\text{M}$  (B). For both compounds the values of  $k_{obs}$  diminish hyperbolically with increasing substrate concentration as per competitive model of inhibition.

Compounds **2** and **4** confirmed our hypothesis about the importance of the carboxylate moiety in modulating affinity and potency to KPC-2 specifically with respect to other related carbapenemases (unpublished). Their ability to interact with the carboxylate-binding pocket defined by Arg-220, Ser-130, Thr-237 and Thr-235 renders them stronger inhibitors compared to lead **1**.

To investigate the ability of designed derivatives **2** and **4** to cross the outer membrane reaching the periplasmic space, where KPC-2 is secreted and confined in Gram negative bacteria, thus synergically preventing  $\beta$ -lactam antibiotics hydrolysis by KPC-2, double disc interaction assays were carried out on *E. coli* overexpressing *bla*<sub>KPC-2</sub> gene. An *E. coli* BL21(DE3) strain, not harboring *bla*<sub>KPC-2</sub> gene, therefore susceptible, was used as control (Figure 5). The synergic effect of **2** and **4** was tested in combination with the antibiotics amoxicillin (AMX), its combination with clavulanic acid (AMC), third generation cephalosporin cefotaxime (CTX), monobactam, aztreonam (ATM) and the carbapenems imipenem (IMP) and meropenem (MEM) (see supplemental material).

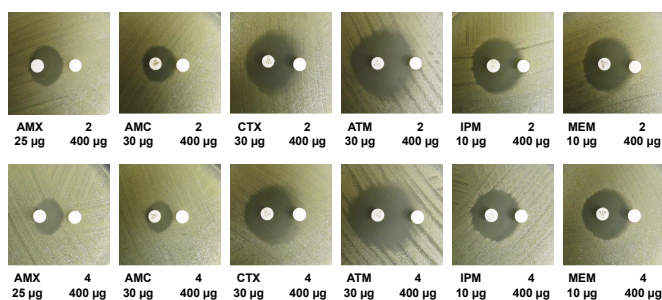


**Figure 5.** Disk Diffusion Susceptibility Tests for compounds **2** and **4** in combination with AMX, AMC, CTX, ATM, IMP and MEM. Synergic activity can be ascertained when the inhibition zones around any of the antibiotic discs are augmented in the direction of the disc containing the compounds of interest.

The *E. coli* overexpressing *bla*<sub>KPC-2</sub> gene was not susceptible to AMX and AMC while a certain antibiotic effects was observed with CTX, MEM, AZT and IMP (see supplemental information). However, in combination with the above antibiotics, **2** and **4** synergized with all tested antibiotics in the *E. coli* strain producing KPC-2 while **1** did not exert any synergistic effect when tested in association with antibiotics AMX and AMC, at least at the concentration employed in the disk diffusion tests (Figure 5; for additional information see supplemental material). In their combination with AMX, AMC, CTX, ATM, IMP and MEM, **2** and **4** potentiate antimicrobial activity as demonstrated by the increasing in inhibition zones between antibiotics and compounds. The addressed synergistic effect confirms the ability for **2** and **4** to reach the periplasmic space of Gram (-) bacteria, preventing  $\beta$ -lactam antibiotics degradation by KPC-2. The synergic effect of **2** and **4** with AMX and AMC is much more evident than with other antibiotics. As a matter of fact, KPCs hydrolyze carbapenems, cefotaxime and aztreonam less efficiently than penicillins and narrow-spectrum cephalosporins.<sup>[12]</sup>

For **1**, **2** and **4** MICs by a two-dimensional checkerboard microdilution assay and drug interactions model via the

fractional inhibitory concentration index (FICI) were determined against *E. coli*-*bla*<sub>KPC-2</sub> (Table 3) and six clinical isolates of *Klebsiella pneumoniae* expressing (4 isolates) or not (2 isolates) KPC-2 (Table 4). Noteworthy, none of the tested compounds had intrinsic antibiotic activity (MIC >256  $\mu$ g/mL) against employed strains, including the susceptible ones.<sup>[17, 22]</sup>

Obtained results confirm synergistic activity and quantify the synergistic effect when present, thus further validating our optimized leads (Table 3, Table 4).

Results against *E. coli*-*bla*<sub>KPC-2</sub> show, first of all, that our phenyl boronic acids act with a synergic mechanism, with only two exceptions, represented by **1**- and **4**-CTX combination having a FIC index slight above 0.5 (indifference) (Table 3).

As far as potency is concerned, **2** and **4** always exert a stronger synergistic activity compared to starting compound **1**.

While for **1** the MIC improvements, for compound concentration ranging from 128 to 16  $\mu$ g/mL, resulted between 2 and 32 fold in the best case (i.e. in combination with MEM, 32 fold improvement at 16  $\mu$ g/mL), for **2** and **4** MIC reduction was more dramatic and at concentrations ranging from 32 down to 0.25  $\mu$ g/mL for **2** and from 4 to 0.5  $\mu$ g/mL for **4** (Table 3).

Compound **2** reduces MICs by a factor of 32 when in combination with AMC and AMX at a concentration as low as 0.25  $\mu$ g/mL. In combination with ATM the reduction is >16 fold at 32  $\mu$ g/mL and, very promising, by a factor of 16 when in association with last resort carbapenem MEM at just 0.25  $\mu$ g/mL. Moreover compound **2** resulted synergic also in combination with CTX, while **1** and **4** did not.

Results for **4** were very promising as well. Compound **4** reduces MICs by 64 fold when in combination with AMC and AMX at 2 and 4  $\mu$ g/mL concentrations respectively. Moreover it reduces MIC by a factor of 32 when in combination with MEM at 0.5  $\mu$ g/mL concentration, showing comparable potency as **2** when in association with last resort carbapenem (Table 3).

Steaming from these encouraging results compounds **1**, **2** and **4** were further tested for their synergistic activity against a set of KPC-2 overproducing clinical isolates. MEM was chosen as the antibiotic considering the synergistic effects exerted by all compounds when in combination with it (Table 3).

The six *K. pneumoniae* clinical strains used in this study were isolated from different patients at the Hospital Universitario Son Espases, Palma de Mallorca, Spain. Two out of six clinical strains were not KPC-2 producers and were susceptible to meropenem (strains 1-2; MIC <0.25  $\mu$ g/mL). In turn four strains harbored *bla*<sub>KPC-2</sub> gene and were resistant to MEM (strains 3-6) (Table 4).

All compounds showed clear synergisms with MEM against the four resistant strains, except compound **1** against strain 6. The obtained results were very encouraging: while all compounds were capable of reducing MIC when in association with MEM, including starting compound **1** (MIC reduction between 16 to 64 fold at 4  $\mu$ g/mL), compounds **2** and **4** were active at concentration as low as 1  $\mu$ g/mL reducing MIC in most cases by 1024 fold, thus restoring bacterial susceptibility to meropenem (MEM) (Table 4).

**Table 3.** *In vitro* interaction between antibiotics and boronic compounds determined by FICI vs *E.coli*-*bla*<sub>KPC-2</sub>.

Checkerboard microdilution assays and Drug interaction model						
Compound	Antibiotic	MIC <sup>[a]</sup> antibiotic ( $\mu\text{g/mL}$ )	MIC <sup>[a]</sup> combination ( $\mu\text{g/mL}$ )	Inhibitor concentration ( $\mu\text{g/mL}$ )	$\Sigma\text{FIC}_{\text{min}}$	FIC Index <sup>[b]</sup> INT
<b>1</b>	AMC	128/64	16/8 8/4	32 64	<0.1875 <0.1875	SYN SYN
	AMX	>16384	512	32	<0.0938	SYN
	ATM	>64	32 16	64 128	<0.3750 <0.3750	SYN SYN
	CTX	512	256	16	<0.5313	IND
	MEM	2	0.0625	16	<0.0626	SYN
	<b>2</b>	AMC	64/32	2/1	0.25	<0.0318
AMX		8192	256	0.25	<0.1255	SYN
ATM		>64	4	32	<0.0938	SYN
CTX		256	64	128	<0.5	SYN
MEM		1	0.0625	0.25	<0.0630	SYN
<b>4</b>	AMC	128/64	2/1	4	<0.0234	SYN
	AMX	16384	256	2	<0.0195	SYN
	ATM	>64	64	0.5	<0.0166	SYN
	CTX	512	256	0.5	<0.5010	IND
	MEM	2	0.0625	0.5	<0.0323	SYN

<sup>[a]</sup> MIC values were determined as the median of three independent experiments. <sup>[b]</sup> INT, interpretation; IND, indifference; SYN, synergy; ANT, antagonism. Synergy is defined when the FICI is  $\leq 0.5$ , antagonism when the FICI is  $> 4$ , and indifference when the FICI is  $> 0.5$  and  $\leq 4$ .

### Cell viability Assays

Cell viability against mouse embryonic fibroblasts (MEFs) and human CCD-Lu34 (CCD) cells was determined for compound **1** (data not shown) and for most active compounds **2** and **4** via a tetrazolium salt (MTT) assay reduction assay (Figure 6).<sup>[33]</sup> After a 24-h exposure to compound **2** no general cytotoxicity was detected at 50  $\mu\text{M}$  (116 fold the  $K_i$ ) against both tested cellular lines: 86% and 88% of cell viability against MEFs and human CCD-Lu34 cells respectively. For compound **4** after a 24-h exposure no general cytotoxicity was detected at 25  $\mu\text{M}$  (176 fold the  $K_i$ ): 93% and 97% of cell viability against MEFs and human CCD-Lu34 cells respectively. For compound **2** cell survival gets down to 37% for MEFs and to 54% for CDD only when compound reached a concentration 700 fold the  $K_i$ ; while for compound **4** at 150  $\mu\text{M}$  (over 1000 fold the  $K_i$ ) cell survival was still stable at 75 % respect to non-exposed cells (Figure 6). In conclusion cell viability assays did not show a significant decrease in viability for cell lines grown in the presence of either compound **2** or **4** while viability was strongly affected by DMSO used as positive control.

### Crystal structures of KPC-2\_compound 2 and KPC-2\_compound 4 complexes.

Compounds **2** ([2-(2-carboxyvinyl)phenyl]boronic acid) and **4** ([2-(2-carboxyethyl)phenyl]boronic acid) binding orientation in KPC-2 were experimentally determined via X-ray crystallography. As

already reported,<sup>[28]</sup> a minor truncation of the C-terminus of KPC-2 was implemented, resulting in improved crystal growth and diffraction quality.

The structure of the EcKpc-2:2 complex was determined to a resolution of 1.4 Å. In addition to **2**, 154 water molecules and 3 ethylene glycol molecules were included and the final model refined to an R (work) value of 17.7% and an R (free) value of 18.5%. Analogously, high resolution structure of EcKpc-2:4 complex was obtained by soaking techniques (1.5 Å). The final model was refined to 15.9% R(work) value and 18.3% R(free) including **4** and 384 water molecules. In both cases, the electron density clearly shows the presence of the inhibitor trapped into the active site, covalently bound to catalytic Ser-70.

First of all, **2** and **4** form a covalent bond, via its boron atom, with the  $\text{O}_\gamma$  atom of Ser-70. Both boronate oxygens interact extensively: boronic acid O2 oxygen establishes multiple hydrogen bonds with the catalytic base Glu-166, backbone NH of catalytic Ser-70 and Asn-170 sidechain, while boronic acid O1 oxygen hydrogen binds backbone CO and NH of Thr-237 and backbone NH of catalytic Ser-70 as well. Overall, derivative **2** as well as derivative **4** adopts a deacylation transition-state analogue conformation with inverted boron configuration. In such a conformation, previous described for other class A BLs, the positions of the boronic acid oxygens are the following: one is located in the oxyanion hole and the other one displaces the

**Table 4.** *In vitro* interaction between antibiotics and boronic compounds determined by FICI vs *K. pneumoniae* clinical strains.

Checkerboard microdilution assays and Drug interaction model vs <i>Klebsiella pneumoniae</i> clinical strains							
Compound	Clinical Strains	MIC <sup>[a]</sup> MEM ( $\mu\text{g/mL}$ )	MIC <sup>[a]</sup> compound ( $\mu\text{g/mL}$ )	MIC <sup>[a]</sup> combination ( $\mu\text{g/mL}$ )	Inhibitor concentration ( $\mu\text{g/mL}$ )	$\Sigma\text{FIC}_{\text{min}}$	FIC Index <sup>[b]</sup> INT
1	Strain 3	256	$\geq 256$	4	4	<0,023	SYN
	Strain 4	256	$\geq 256$	16	4	<0,0937	SYN
	Strain 5	256	$\geq 256$	4	4	<0,0234	SYN
	Strain 6	$\geq 256$	$\geq 256$	$\geq 256$	256	<1,5	IND
2	Strain 3	256	$\geq 256$	2	1	<0,0117	SYN
	Strain 4	256	$\geq 256$	0.25	1	<0,0015	SYN
	Strain 5	256	$\geq 256$	0.25	1	<0,0015	SYN
	Strain 6	$\geq 256$	$\geq 256$	4	8	<0,0156	SYN
4	Strain 3	256	$\geq 256$	4/2	1	<0,0195	SYN
	Strain 4	256	$\geq 256$	0.25	1	<0,0015	SYN
	Strain 5	256	$\geq 256$	0.25	1	<0,0015	SYN
	Strain 6	$\geq 256$	$\geq 256$	8/4	8	<0,0234	SYN

<sup>[a]</sup> MIC values were determined as the median of two independent experiments, <sup>[b]</sup> INT, interpretation; IND, indifference; SYN, synergy; ANT, antagonism. Synergy is defined when the FICI is  $\leq 0.5$ , antagonism when the FICI is  $> 4$ , and indifference when the FICI is  $> 0.5$  and  $\leq 4$ .

deacylation water normally positioned between Glu-166 and Asn-170.<sup>[27,34]</sup>

Compound **2** orients its phenyl ring against one hydrophobic region defined by Trp-105 and Leu-167 in the proximity of the opening of the binding site. The phenyl ring of **2** is involved in cation- $\pi$  and  $\pi$ - $\pi$  interactions with Asn-132 and Trp-105, respectively. Finally, as expected, **2** orients its *ortho* carboxyvinyl lateral chain towards the C3(4') carboxylate binding pocket, highly conserved in all serine-BLs. In this site, the carboxylate group is trapped in a network of hydrogen bonds with Thr-237, Thr-235, Ser-130 sidechains and a highly conserved water molecule (Wat 99#, Figures 7A-B and Figure 8). Despite the higher degree of freedom of the carboxyethyl *ortho* substituent (**4**), such inhibitor assume a conformation closely overlapping that described above for **2**: the 2-carboxyethyl lateral chain occupies the targeted binding pocket of  $\beta$ -lactam antibiotics C3(4') carboxylate with similar orientation. The highly conserved water molecule (Wat 105#) is also present in the site contributing to the carboxylate chain binding geometry optimization (Figures 9A, 9B and Figure 10<sup>[35]</sup>).

The overall EckKpc-2 protein structure well superposes to the C-term truncated KPC-2 structure in complex with citric acid and to the KPC-2 apoprotein (PDB id 3C5A and 3DW0)<sup>[28]</sup> with r.m.s.d. of 0.45 and 0.21 Å over 264 aligned Ca atoms, respectively (software Gesamt).<sup>[36]</sup> The only significant shift (r.m.s.d. higher than 2 Å) pertains a short loop, from Thr-254 to Arg-256, and it is due to interactions promoted by the crystal packing. Indeed, Arg-256 side chain is clearly rotated if compared to apoprotein

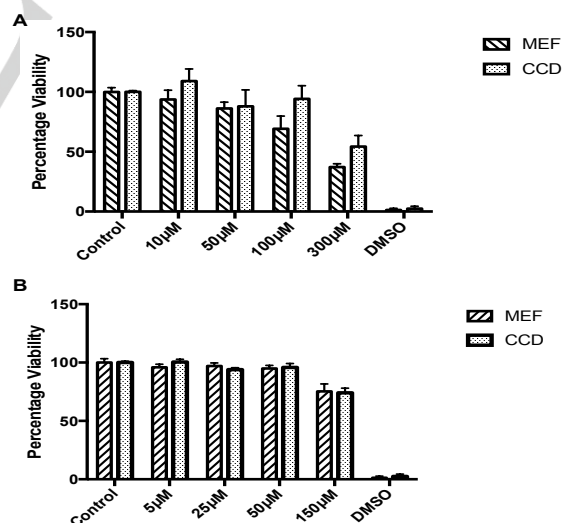


**Figure 6.** Cell proliferation graphics determined by MTT assay after 24 hours incubation with compounds **2** (A) and **4** (B).

and points towards **2** in the active site of a symmetry-related protein molecule. Indeed, Arg-256 orients its cationic sidechain toward such an adjacent active site and establishes interactions with the **2** phenyl ring (cation- $\pi$  interaction) and the main chain carbonyl of Thr-237 (H-bond). Analogous considerations can be deduced for the EckKpc2-**4** complex.

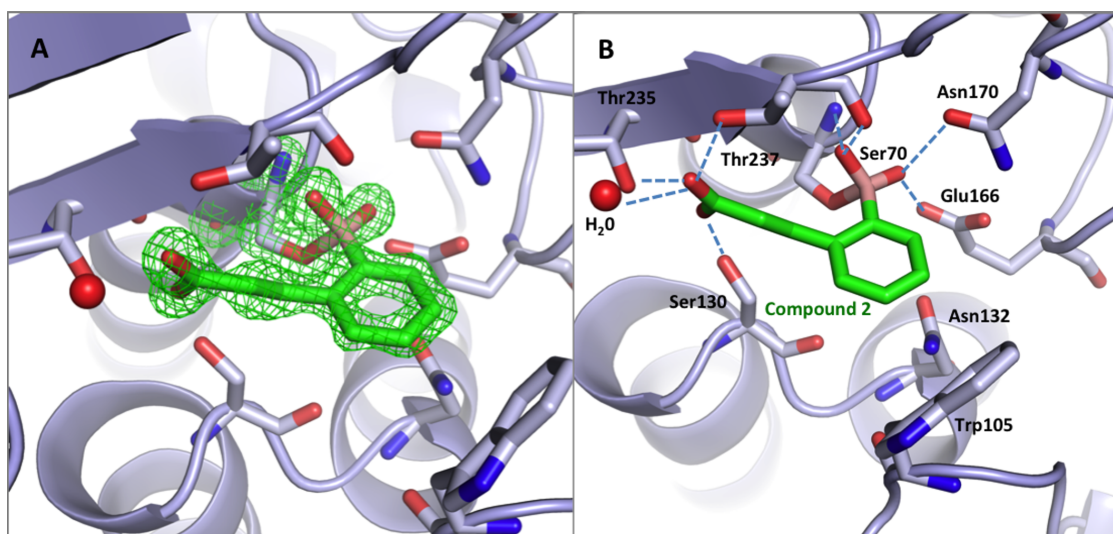


**Figure 7.** Crystal structure of KPC-2 in complex with **2**. (A) omit map (phenix.composite\_omit\_map) is shown (8 $\sigma$  contour level). (B) ligand binding mode and the main residues involved in the ligand-protein interactions are shown as sticks (carbon atoms in green for **2** and in gray for EcKpc-2, oxygen atoms in red, nitrogen in blue, boron atom in pink, water oxygen in cyan). Pictures were prepared using Pymol (The PyMOL Molecular Graphics System, version 1.5.0.4; Schrödinger LLC: New York, 2010; <http://www.pymol.org>).

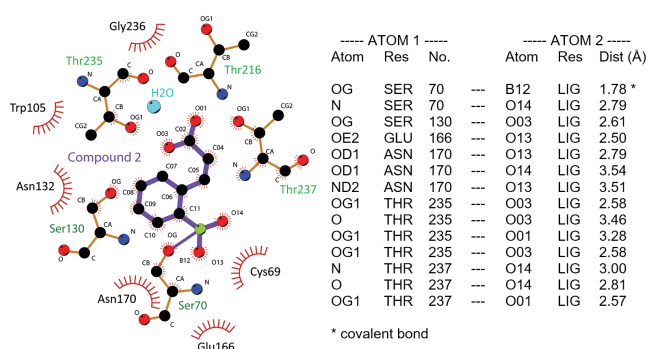


**Figure 8.** Key Interactions KPC-2 and the ligand **2**. Distances between 2.5 and 3.6 Å have been selected for non-covalent bonds and listed. Atoms identification codes are defined in the Ligand binding site plot (Ligplus software).<sup>[35]</sup>

As previously mentioned, the presence of a covalent bond between the boronic group of **2** (and **4**) and the catalytic serine of KPC-2 is clearly visible in the electron density.

The crystallographic data above described are consistent with the kinetics of inhibition where the enzyme isomerization has been experimentally determined by the direct observation of the distinctive saturable function of  $k_{\text{obs}}$  versus the inhibitor concentration.

The boronic derivatives **2** and **4** lead to the formation of a relatively stable transition-state analogue passing through an initial encounter complex.

The slow-reversible nature of the inhibition for **2** and **4** is therefore, the consequence of the non-zero value of the rate constant  $k_{-2}$ , while the time-dependence is due to the low value of  $k_{+2}$  rate constant, which is in turn, the consequence of the isomerization step. All these features contribute, *de facto*, to the formation of two inhibitor-enzyme complexes characterised by two different inhibition constants,  $K_i$  and  $K_i^*$ . The last one

represents the inhibition constant of the high affinity complex. The determined values of  $K_i^*$  for **2** and its close analogue **4** are very similar ( $K_i^*$  0.43 and 0.14  $\mu\text{M}$  respectively) as well as their binding orientations in KPC-2 (Figures 7B and 9B).<sup>[31,32]</sup>

The *meta* isomers **3** and **5** behaved differently. As confirmed by the kinetics of inhibition, they act as fully reversible inhibitors, characterised by the only inhibition constant of the Michaelis complex *EI*. It is clear that they do not meet the requirements for the formation of a measurable and stable transition-state, since their mechanism of inhibition conforms to a simple reversible scheme ( $E+I=EI$ ).<sup>[31]</sup>

## Conclusions

Starting from a known phenyl boronic acid with low synergic activity towards organisms overexpressing KPC-2 carbapenemase and through a multidisciplinary approach including design, synthesis, kinetic and X-ray crystallography we identified and validated two nanomolar KPC-2 inhibitors.

Their kinetic description as derivatives acting as time dependent, slow reversible inhibitor of KPC-2 has been deeply investigated. In the derivatization of the phenyl boronic acid, the introduction in *ortho* position of a carboxylated lateral chain strongly improved affinity to KPC-2 (**2** and **4**) while for the *meta* derivatives, (**3,5**) the lateral chain was detrimental for activity underlying the importance of an optimal rearrangement of the carboxylate moiety. Undoubtedly, in derivatives **2** and **4**, the improved affinity to KPC-2 is completely attributable to the additional hydrogen bond in the  $\beta$ -lactam carboxylate binding pocket as confirmed by X-ray crystallography.<sup>[17,37,38]</sup>

Moreover, respect to the starting derivative **1**, in the designed *ortho* derivatives **2** and **4** we have clearly potentiated the *in vitro* antimicrobial activity of a number of  $\beta$ -lactam antibiotics, including the last resort meropenem. Noteworthy, in clinical isolates, derivatives **2** and **4** at 1  $\mu\text{g/mL}$  in combination with meropenem were able to reduce MIC by 1024 fold down to 0.25

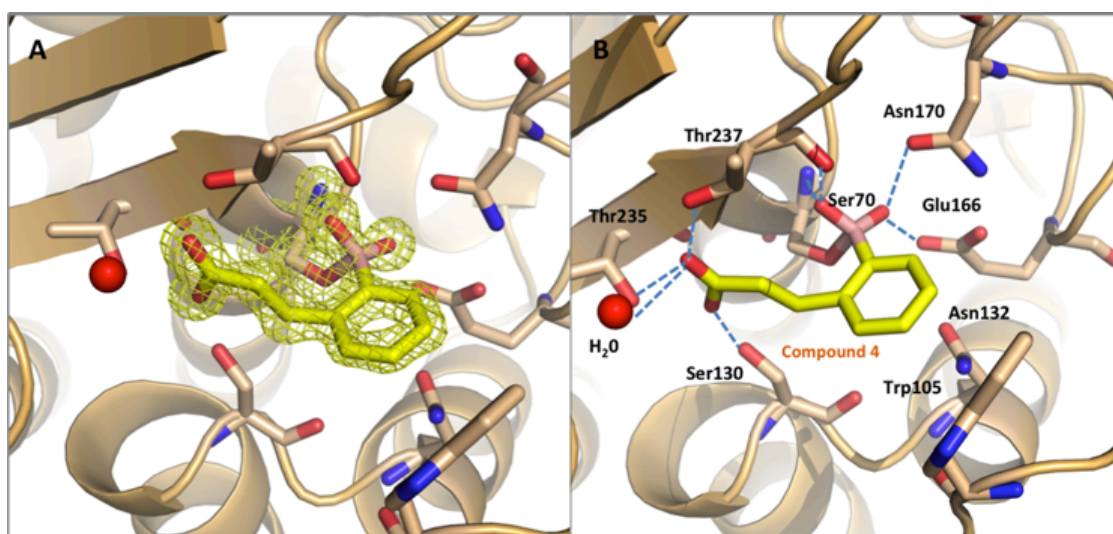


**Figure 9.** Crystal structure of KPC-2 in complex with **4**. (A) omit map (phenix.composite\_omit\_map) is shown (8 $\sigma$  contour level). (B) ligand binding mode and the main residues involved in the ligand-protein interactions are shown as sticks (carbon atoms in yellow for the **4** and in pale orange for the protein, oxygen atoms in red, nitrogen in blue, boron atom in pink, water oxygen in cyan). Pictures were prepared using Pymol (The PyMOL Molecular Graphics System, version 1.5.0.4; Schrödinger LLC: New York, 2010; <http://www.pymol.org>).

$\mu\text{g/mL}$ , restoring completely susceptibility. In turn no cytotoxicity was detected in cell viability assays.

Our small boronic acid derivatives have been clear validated as lead-like KPC-2 inhibitors and undoubtedly the high-resolution structures of KPC-2 in complex with **2** and **4** represent a starting point for future drug design and optimization efforts.

In the here-exploited lead identification and validation we chose to focus on carbapenemases inhibitors, taking advantage of critical consensus binding sites shared by other therapeutically important groups of carbapenemases and BLs: by targeting common hot spots our inhibitors could be further developed as broad-spectrum inhibitors. Further studies are under way with the aim to optimize affinity and spectrum of action vs other serine based carbapenemases.

## Experimental Section

**Chemistry:** Reagents were purchased from Sigma-Aldrich and were of reagent grade. Phenyl boronic acid (**1**) was purchased from Sigma-Aldrich while [2-(2-carboxyvinyl)phenyl]boronic acid (**2**) and [3-(2-carboxyvinyl)phenyl]boronic acid (**3**) were purchased from Alfa Aesar (Table 1). [2-(2-carboxyethyl)phenyl]boronic acid (**4**) and [3-(2-carboxyethyl)phenyl]boronic acid (**5**) were synthesized starting from [2-(2-carboxyvinyl)phenyl]boronic acid (**2**) and [3-(2-carboxyvinyl)phenyl]boronic acid (**3**) respectively through catalytic hydrogenation under H<sub>2</sub> (21 psi) in EtOH using Pd-C 10% as catalyst. Catalytic hydrogenation was conducted in a Parr stirred reactor at room temperature for 5 hours. Reactions progress was monitored by TLC on precoated silica gel 60 F254 plates (Merck). The catalyst was removed by filtration and the solvent removed under vacuum and residue washed with diethyl ether, producing **4** and **5** as white crystalline solid (Table 1). All compounds, both commercially available and in house synthesized (Table 1) were characterized through monodimensional NMR, HR-ESI monoisotopic MS analysis and melting point. NMR spectra were recorded on a Bruker 400 spectrometer with <sup>1</sup>H at 400.134 MHz, <sup>13</sup>C at 100.62 MHz and <sup>11</sup>B at 128 MHz. Proton chemical shift was referenced to the TMS internal standard. Chemical shifts are reported in parts per million (ppm,  $\delta$  units). Mass spectra were obtained on a 6520 Accurate-Mass Q-TOF LC/MS and 6310A Ion TrapLC-MS(n). The melting points were recorded on a Stuart, SMP3 (Barloworld Scientific Limited Stone, Staffordshire, UK) and were uncorrected. The structures of all compounds were consistent with their analytical and spectroscopic data (see supplemental information, Table S1, NMR spectra).

**Cloning of bla<sub>KPC-2</sub>:** The bla<sub>KPC-2</sub> gene was kindly provided by Prof. Sergei Vakulenko (University of Notre Dame du Lac, Indiana, USA). The gene was amplified by PCR using the reported oligonucleotides (see supplemental information, Table S2). The gene encoding the full-length protein has been used for kinetic and antimicrobial susceptibility assays, while the C-terminus deleted form<sup>[28]</sup> has been used for crystallographic studies. KPC-2<sub>for</sub> (BamHI restriction site) and KPC-2<sub>rev</sub> (HindIII restriction site) were used to clone the full-length gene into the pET-24a vector (Novagen). The truncated form of KPC-2 was cloned as the full-length using KPC-2<sub>rev\_del</sub> containing HindIII restriction site and a stop codon, 12 nucleotides upstream the natural end of bla<sub>KPC-2</sub> gene.<sup>[28]</sup> The PCR products were double digested by BamHI and HindIII (Biolabs, New

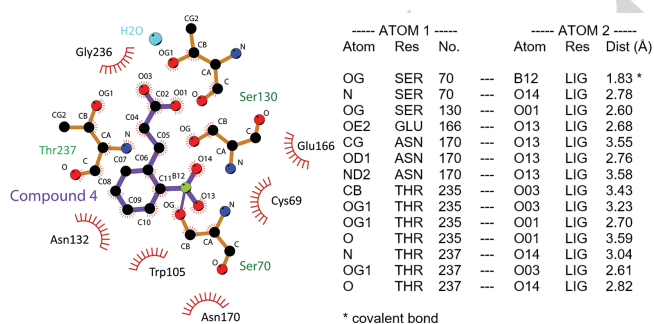


**Figure 10.** Key Interactions KPC-2 and the ligand **4**. Distances between 2.5 and 3.6 Å have been selected for non covalent bonds and listed. Atom identification codes are defined in the Ligand binding site plot (Ligplus software).<sup>[35]</sup>

England), ligated and subsequently transformed into competent *Escherichia coli* HB101. Transformed colonies were selected on Luria Bertani (LB) agar plate (50 mg/mL kanamycin). Clones were confirmed by colony PCR and DNA sequencing using T7\_for and T7\_term oligonucleotides.

**Expression and purification of recombinant KPC-2:** Recombinant plasmids were transformed into competent *E.coli* BL21 (DE3) cells for protein expression. 50 mL of Tryptic Soy Broth (TSB) (50 mg/L kanamycin) were inoculated with fresh colonies and grown at 37°C. 4 mL of the overnight culture were used to inoculate 1.3 L of TSB (50 mg/L kanamycin) grown at 37°C with shaking 0.5 optical density at 600 nm. Expression of recombinant *bla* gene was induced by adding 1.0 mM IPTG (isopropyl-D-thiogalactopyranoside) and the cells were again allowed to grow at 20 °C overnight. Bacteria were harvested by centrifugation at 4000 rpm for 20 minutes. The pelleted cells were resuspended in Tris-HCl 50 mM pH 7.4-7.5. Periplasmic proteins were extracted as reported in pET System Manual (TB055 10th Edition Rev. B 0403) and subsequently dialyzed in sodium acetate buffer (50 mM, pH 5.0). Proteins were conveniently purified in a single step using a Macro-Prep High S resin and eluted using sodium acetate 50 mM pH 5.0 and a sodium chloride (NaCl) linear gradient from 100 to 500 mM. Purified proteins were dialyzed overnight in sodium phosphate buffer 50 mM, pH 7.0.<sup>[29]</sup>

**Steady state enzyme kinetic measurements and determination of inhibition constants:** Kinetic parameters of full-length KPC-2 enzyme against the reporter substrate nitrocefin were determined by monitoring the variation in the absorbance at 482 nm in 50 mM phosphate buffer (PB) (pH 7.0) at 25°C. All measurements were carried on Lambda 2 spectrophotometer (Perkin Elmer). The steady-state kinetic parameter  $K_M$  was determined by non-linear least-square fit of the Michaelis – Menten equation using OriginPro 8.5.1.

**Determination of  $IC_{50}$  and inhibitor reversibility:** The half maximal inhibitory concentration ( $IC_{50}$ ) of boronic acid derivatives was determined as follows. Boronic acids were dissolved in dimethyl sulfoxide (DMSO) to a concentration of 10 mM and stored at -20°C. Each compound was tested at concentrations ranging from 1  $\mu$ M to 500  $\mu$ M for inhibitory activity vs full-length KPC-2 enzyme (3.1 nM) in 50 mM of PB at pH 7.0 at 25°C in the presence of nitrocefin as the reported substrate. Nitrocefin hydrolysis was followed at 482 nm. All the experiments were performed in triplicate. Experimental error never exceeds 5% (Table 1). The reversibility of inhibition for each derivative was determined as well. KPC-2 was incubated at 25°C for 10 minutes at a concentration of 100-fold over the concentration required for the activity assay, with a concentration of inhibitor about 5-fold the  $K_i$  estimated from the previously determined  $IC_{50}$  values. After the pre-incubation time, the recovery of the enzymatic activity was determined after rapid and large dilution, (100-fold) of the enzyme-inhibitor complex, with the reaction buffer (PB 50 mM, pH 7.0) containing the reporter substrate nitrocefin at 180  $\mu$ M.<sup>[30]</sup> The time-course of nitrocefin hydrolysis was followed at 482 nm (Figure 2).

**Time dependent inhibitors:** For compounds behaving as reversible time-dependent inhibitors (**2** and **4**) the time course curve, for reactions monitored at fixed concentrations of enzyme, reporter substrate and slow binding inhibitor, is described by the following equation:

$$[P] = v_{ss}t + \frac{v_i - v_{ss}}{k_{obs}}(1 - e^{-k_{obs}t}) \quad (A.1)$$

where  $v_{ss}$  is the steady-state velocity,  $v_i$  the initial velocity and  $k_{obs}$  the rate constant for conversion from the initial to the steady-state velocity. Fitting of a progress curve to equation A.1, allows the estimation of  $v_i$ ,  $v_{ss}$  and  $k_{obs}$ .

The plot showing the dependence of  $k_{obs}$  on inhibitor concentration is useful to distinguish between simple reversible slow binding inhibitor and

the inhibitory mechanism involving enzyme isomerization step. In the latter case the scheme of reaction is:



The scheme describes a two-step binding mechanism where a first step is characterized by a rapid equilibrium binding of the inhibitor to the enzyme to form the encounter complex (*EI*) and a second step characterized by a slow isomerization of the enzyme to form the high affinity complex (*EI\**).

The value of  $k_{obs}$  for this mechanism is a saturable function of inhibitor concentration (Figures 3A and 3B) and can be describe by the following equation:

$$k_{obs} = k_{-2} + \left( \frac{k_{+2}[I]}{K_i^{app} + [I]} \right) \quad (A.3)$$

$k_{-2}$  can be estimated as the intercept of the hyperbolic curve when the concentration of the inhibitor is equal to zero. The horizontal asymptote of the curve represents the maximum value of  $k_{obs}$  ( $k_{max}$ ) which is:

$$k_{max} = k_{+2} + k_{-2} \quad (A.4)$$

For the enzyme isomerization mechanism, as described in equation A.2, two apparent constants of inhibition can be defined:  $K_i^{pp}$  for the initial inhibitor encounter complex (*EI*), and  $K_i^{app}$  for the final high-affinity conformation (*EI\**).

The value of  $K_i^{app}$  is calculated as the concentration of the inhibitor yielding the half value of  $k_{max}$ .

When the inhibitor behaves as competitive, the values of  $K_i$  are calculated by Cheng-Prusoff equations:

$$K_i^{app} = K_i \left( 1 + \frac{[S]}{K_M} \right) \quad (A.5)$$

$K_i^{app}$  can be obtained as the half-maximal concentration of the plot  $v_{ss}/v_0$  (where  $v_0$  is the initial rate of the uninhibited reaction) as a function of the decimal logarithm of the inhibitor concentrations (Figures 3C and 3D).  $K_i^*$  can be obtained by the following equation:

$$K_i^* = \frac{K_i}{1 + (k_{+2}/k_{-2})} \quad (A.6)$$

All the experiments were performed at 25°C in PB 50 mM, pH 7.4 using nitrocefin at 180  $\mu$ M (5-fold the  $K_M$  value).

The mechanism of inhibition for the time-dependent inhibitors can be determined by measuring the effects of reporter substrate concentration on  $k_{obs}$  value at fixed inhibitor concentration. For a competitive inhibitor the value of  $k_{obs}$  will decrease hyperbolically with increasing substrate concentration (Figure 4A and 4B).<sup>[31,32]</sup>

The experiment was conducted in PB 50 mM, pH 7.4 at 25°C using nitrocefin as the reporter substrate at concentrations ranging from 10 to 350  $\mu$ M (about 0.3-fold to 10-fold the  $[S]/K_M$  ratio) and compounds **2** and **4** at fixed concentration of 12  $\mu$ M and 6  $\mu$ M, respectively (about 5-fold the  $K_i$  values).

All the experiments were performed in triplicate. Experimental error never exceeds 5%. All the kinetic parameters and the non-linear fitting were calculated using the software OriginPro 8.5.1.

**Double Disk diffusion assay:** The antimicrobial susceptibility of *E.coli* BL21 (DE3) pET-24a-*bla*<sub>KPC-2</sub> versus amoxicillin (AMX), amoxicillin/clavulanic acid (AMC), cefotaxime (CTX), aztreonam (AMT), and meropenem (MEM) (Oxoid) in combination with **1**, **2** and **4** were investigated by double disc diffusion assay (Figure 5). 400  $\mu$ g of each boronic acid derivative were dispensed individually on sterile blank filter paper disc (Oxoid). The maximum amount of DMSO (dimethyl sulfoxide) used to dissolve the phenyl boronic acid derivatives (26.86  $\mu$ g) was also tested for control (see supplemental information). Discs were placed on

MH Agar plates inoculated with  $5 \times 10^5$  CFU/mL of bacterial suspension at a distance equal to the half measured inhibition diameter for each drug alone. *E. coli* (DE3) pET-24a, without *bla*<sub>KPC-2</sub> gene, was used as control. The plates were incubated 18 hours at 37°C and the inhibition diameters, in millimeters, were measured. Additional data and figure are available as supplemental information.

**Checkerboard microdilution assay:** The *in vitro* interactions between the antibiotics used for the double disk assay and the boronic compounds were investigated by a two-dimensional checkerboard microdilution assay, using a 96-well microtitration plates as previously described.<sup>[39]</sup> Assays were conducted against the *E. coli* BL21 (DE3) pET-24a-*bla*<sub>KPC-2</sub> and against six *K. pneumoniae* clinical strains isolated from different patients at the Hospital Universitario Son Espases, Palma de Mallorca, Spain. The microtiter plates were incubated at 37°C for 18 hours. The growth in each well was quantified spectrophotometrically at 595 nm by a microplate reader iMark, BioRad (Milan, Italy). The percentage of growth in each well was calculated as:

$$\frac{OD_{drug\ combination\ well} - OD_{background}}{OD_{drug\ free\ well} - OD_{background}}$$

where the background was obtained from the microorganism-free plates, processed as the inoculated plates. The MICs for each combination of drugs were defined as the concentration of drug that reduced growth by 80% compared to that of organisms grown in the absence of drug.

**Drug interaction models:** To assess the nature of the *in vivo* interactions between the compounds and antibiotics against *E. coli* BL21 (DE3) pET-24a-*bla*<sub>KPC-2</sub> and six *K. pneumoniae* clinical strains, the data obtained from the checkerboard assay were analyzed in order to calculate the fractional inhibitory concentration index.<sup>[40]</sup>

The fractional inhibitory concentration index (FICI), is the mathematical expression of the effect of the combination of antibacterial agents expressed as:

$$\Sigma FIC = FIC_A + FIC_B = \frac{MIC_{AB}}{MIC_A} + \frac{MIC_{BA}}{MIC_B}$$

where  $MIC_A$  and  $MIC_B$  are the MICs of drugs A and B when acting alone and  $MIC_{AB}$  and  $MIC_{BA}$  are the MICs of drugs A and B when acting in combination. Among all  $\Sigma FIC$ s calculated for each microplate, the FICI was determined as the lowest  $\Sigma FIC$  ( $\Sigma FIC_{min}$ ) when synergy is supposed, or the highest  $\Sigma FIC$  ( $\Sigma FIC_{max}$ ) when antagonism is evident. Since in MIC determination, the variation in a single result places a MIC value in a three-dilution range ( $\pm 1$  dilution), the reproducibility errors in MIC checkerboard assays are considerable.

For that reason, the interpretation of FICI data should be done taking into consideration values well below or above the theoretical cut-off (1.0) defined by Berenbaum. Synergy was, therefore, defined when  $FICI \leq 0.5$ , while antagonism was defined when  $FICI > 4$ . A FIC index between 0.5 and 4 ( $0.5 < FICI \leq 4$ ) was considered indifferent.<sup>[41]</sup>

**Cell viability assay:** Cell viability was determined with the 3-[4,5-dimethylthiazol-2-yl]-2,5-diphenyltetrazolium bromide (MTT) reduction assay. Mouse embryonic fibroblasts (MEFs) and human CCD-Lu34 cells were seeded ( $8 \times 10^4$ ) in 96-well plates and allowed to attach overnight.<sup>[33]</sup> The day after, cells were treated with the indicate concentrations of compounds **2** and **4** for 24 hours. At different time points, cells were incubated for 3 hours at 37 °C with MTT (0.5 mg/mL in phosphate-buffered saline (PBS)). The formazan crystals were dissolved by adding 100  $\mu$ L of stop solution (90% 2-propanol, 10% Dimethyl sulfoxide (DMSO)) to each well followed by quick mixing. After 15 min, the absorbance at 595 nm was estimated using a plate reader (Tecan Infinite® M200 PRO). Cells not treated with the compounds were considered as negative control while cells treated with 15% DMSO were used as positive control of cytotoxicity.

**Crystallization, Data Collection and Structures determination of EckKPC-2 in complex with 2 and 4:** For crystallization purposes, KPC-2 was further purified using a Superose 12 10/300GL column (GE Helthcare) equilibrated in 40 mM Bis-Tris pH 5.9 and subsequently concentrated by ultrafiltration to 20 mg/mL in the same buffer. EckKPC-2:2 and EckKPC-2:4 complex crystals were obtained by soaking techniques. The apo EckKPC-2 crystals were grown in 15% polyethylene glycol 6000 (PEG 6000) in 200 mM potassium thiocyanate (KSCN) and 100 mM sodium citrate (pH 4) at 20°C using the vapor diffusion hanging drop method. Crystals appeared after one week. KPC-2 crystals were soaked for 2-3 hours at 20°C with **2** or **4** (3 mM) dissolved into reservoir solution. The compound solution was prepared by mixing reservoir solution and a 50 mM stock solution of **2** or **4** in DMSO. For data collection, the crystals were back washed in cryoprotectant solution (reservoir solution supplemented with 20% ethylene glycol), left equilibrating for 30 seconds and flash-frozen in liquid nitrogen. X-ray diffraction data were collected at the beamline id23eh1 and id23eh2 of the European Synchrotron Radiation Facility (ESRF, Grenoble). EckKPC-2:2 and EckKPC-2:4 crystals diffracted up to 1.4 and 1.5 Å maximum resolution, respectively. Data sets were integrated, scaled and truncated through the automated processing pipeline feasible at ESRF MX beamlines and further evaluated by data reduction software.<sup>[42,43]</sup> The phase problem was solved by molecular replacement with PHASER 2.6.0.<sup>[44]</sup> *E. coli* KPC-2 structure as template (PDB id 3C5A).<sup>[28]</sup> Final structure was obtained by refinement cycles using Refmac5 and Refine,<sup>[45]</sup> alternated with manual model rebuilding with Coot molecular graphic software<sup>[46]</sup> through the CCP4i2 interface (CCP4-7.0). In both cases, after few refinement cycles, a clear electron density in the difference maps was observed as a continuous surrounding the catalytic Ser-70 and could be clearly interpreted as the inhibitor molecule, covalently bound to the side chain oxygen of Ser-70. The ligand molecule was built and optimized with Elbow,<sup>[47]</sup> manually fitted in the difference maps using Coot molecular graphic tools and further refined using Refmac5 and Refine.<sup>[45]</sup> Five percent of the X-ray data were used for R-free cross-validation. Pymol and CCP4mg Molecular Graphics software were used to generate illustrations, while composite omit maps with simulated annealing were calculated using Phenix environment maps options (phenix.composite\_omit\_map).<sup>[48]</sup> LIGPLOT/GIANT were used to analyse and visualize protein-ligand interactions (additional data and refinement statistics are available as supplemental information, Table S3.<sup>[35]</sup> The crystallographic data for the binary complexes of KPC-2 with **2** and **4** were deposited in the PDB (accession code: 5LL7 for **2** and 5MGI for **4**).

## Founding

This work was supported by grant FAR2014 (Finanziamento di Ateneo per la Ricerca) from University of Modena and Reggio Emilia to DT supporting independent research on Carbapenemases.

## Acknowledgments

The *bla*<sub>KPC-2</sub> gene was kindly provided by Prof. Sergei Vakulenko of the Notre Dame University of Indiana, USA. The authors thank the Centro Interdipartimentale Grandi Strumenti (CIGS) of Modena for access to its facilities and analytical support. JB and AO were funded by Instituto de Salud Carlos III, Subdirección General de Redes y Centros de Investigación Cooperativa, Ministerio de Economía y Competitividad, the Spanish Network for Research in Infectious Diseases (REIPI RD12/0015) co-financed by European Development Regional Fund 'A way to achieve Europe' ERDF.

## Data Availability

The coordinates and structure factors for the KPC-2-compound 2 and the KPC-2-compound 4 complexes were deposited in the Protein Data Bank (PDB identifiers **5LL7** and **5MGI**, respectively).

## Supplementary data

Supplementary data associated with this article can be found, in the online version, at ----, Table S1. Chemical characterization data for boronic acids derivatives 1-5. Table S2, Oligonucleotides used for cloning blaKPC-2 gene. Table S3 and S4 Double Disk Synergy Assays Interpretative Information. Table S5. Data Collection and Refinement Statistic for binaries complexes 5LL7 and 5MGI. Table S6. In silico properties and ligand efficiencies for starting compound **1** and leads **2** and **4**. <sup>1</sup>H-NMR and <sup>13</sup>C-NMR spectra. Double Disk Synergy Assays pictures.

## Conflict of interest

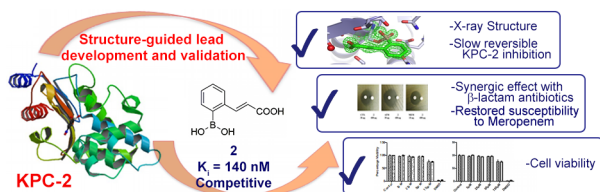
The authors declare no conflict of interest.

**Keywords:** Bacterial Resistance • *Klebsiella Pneumoniae* KPC-2 • X-ray diffraction • clinical strains • cell viability

## References:

- [1] [1] K. M. Papp-Wallace, A. Endimiani, M. A. Taracila, R. A. Bonomo, *Antimicrob. Agents Chemother.* **2011**, *55*, 4943–4960.
- [2] D. Tondi, S. Cross, A. Venturelli, M. P. Costi, G. Cruciani, F. Spyraakis, *Curr. Drug Targets* **2016**, *17*, 983–1005.
- [3] D. M. Livermore, N. Woodford, *Trends Microbiol.* **2006**, *14*, 413–420.
- [4] D. Farina, F. Spyraakis, A. Venturelli, S. Cross, D. Tondi, M. Paola Costi, *Curr. Med. Chem.* **2014**, *21*, 1405–1434.
- [5] J.-M. Frère, E. Sauvage, F. Kerff, *Curr. Drug Targets.* **2016**, *17*, 974–982.
- [6] T. Naas, L. Dortet, B. I. Iorga, *Curr. Drug Targets.* **2016**, *17*, 1006–1028.
- [7] D. Schillaci, V. Spanò, B. Parrino, A. Carbone, A. Montalbano, P. Barraja, P. Diana, G. Cirrione, S. Cascioferro, *Journal of Medicinal Chemistry.* **2017**, *60* (20), 8268–8297
- [8] F. Spyraakis, G. Celenza, F. Marcoccia, M. Santucci, S. Cross, P. Bellio, L. Cendron, M. Perilli, D. Tondi, *ACS Med. Chem. Lett.* **2018**, *9* (1), 45–50
- [9] H. Giamarellou, *Int. J. Antimicrob. Agents* **2010**, *36 Suppl 2*, S50–4.
- [10] D. M. Livermore, S. Mushtaq, M. Warner, J.-C. Zhang, S. Maharjan, M. Doumith, N. Woodford, *J. Antimicrob. Chemother.* **2011**, *66*, 48–53.
- [11] F. Perez, A. Endimiani, A. J. Ray, B. K. Decker, C. J. Wallace, K. M. Hujer, D. J. Ecker, M. D. Adams, P. Toltzis, M. J. Dul, et al., *J. Antimicrob. Chemother.* **2010**, *65*, 1807–1818.
- [12] P. Nordmann, G. Cuzon, T. Naas, *Lancet. Infect. Dis.* **2009**, *9*, 228–236.
- [13] O. Blennow, P. Ljungman, *Br. J. Haematol.* **2016**, *172*, 497–511.
- [14] E. Cerceo, S. B. Deitelzweig, B. M. Sherman, A. N. Amin, *Microb. Drug Resist.* **2016**, *22*, 412–431.
- [15] N. P. Krishnan, N. Q. Nguyen, K. M. Papp-Wallace, R. A. Bonomo, F. van den Akker, *PLoS One* **2015**, *10*, e0136813.
- [16] D. Tondi, R. A. Powers, E. Caselli, M. C. Negri, J. Blazquez, M. P. Costi, B. K. Shoichet, *Chem. Biol.* **2001**, *8*, 593–611.
- [17] D. Tondi, A. Venturelli, R. Bonnet, C. Pozzi, B. K. Shoichet, M. P. Costi, *J. Med. Chem.* **2014**, *57*, 5449–5458.
- [18] A. Venturelli, D. Tondi, L. Cancian, F. Morandi, G. Cannazza, B. Segatore, F. Prati, G. Amicosante, B. K. Shoichet, M. P. Costi, *J. Med. Chem.* **2007**, *50*, 5644–5654.
- [19] D. Tondi, S. Calo, B. K. Shoichet, M. P. Costi, *Bioorg. Med. Chem. Lett.* **2010**, *20*, 3416–3419.
- [20] L. J. Rojas, M. A. Taracila, K. M. Papp-Wallace, C. R. Bethel, E. Caselli, C. Romagnoli, M. L. Winkler, B. Spellberg, F. Prati, R. A. Bonomo, *Antimicrob. Agents Chemother.* **2016**, *60*, 1751–1759.
- [21] J. P. Werner, J. M. Mitchell, M. A. Taracila, R. A. Bonomo, R. A. Powers, *Protein Sci.* **2017**, *26*, 515–526.
- [22] M. Santucci, F. Spyraakis, S. Cross, A. Quotadamo, D. Farina, D. Tondi, F. De Luca, J. D., Docquier, A. Prieto, C. Ibacache, J. Blázquez, A. Venturelli, G. Cruciani, M. P. Costi, *Scientific Reports* **2017**, *7*, (1), Article number: 17716. doi:10.1038/s41598-017-17399-7
- [23] J. Brem, R. Cain, S. Cahill, M. A. McDonough, I. J. Clifton, J.-C. Jiménez-Castellanos, M. B. Avison, J. Spencer, C. W. G. Fishwick, C. J. Schofield, *Nature Communications.* **2016**, *7*, 12406.
- [24] D. M. Livermore, S. Mushtaq, *J. Antimicrob. Chemother.* **2013**, *68*, 1825–1831.
- [25] A. L. Hopkins, G. M. Keserü, P. D. Leeson, D. C. Rees, C. H. Reynolds, *Nat. Rev. Drug Discov.* **2014**, *13*, 105–121.
- [26] W. Ke, C. R. Bethel, K. M. Papp-Wallace, S. R. R. Pagadala, M. Nottingham, D. Fernandez, J. D. Buynak, R. A. Bonomo, F. van den Akker, *Antimicrob. Agents Chemother.* **2012**, *56*, 2713–2718.
- [27] N. Q. Nguyen, N. P. Krishnan, L. J. Rojas, F. Prati, E. Caselli, C. Romagnoli, R. A. Bonomo, F. van den Akker, *Antimicrob. Agents Chemother.* **2016**, *60*, 3, 1760–1766.
- [28] S. Petrella, N. Ziental-Gelus, C. Mayer, M. Renard, V. Jarlier, W. Sougakoff, *Antimicrob. Agents Chemother.* **2008**, *52*, 3725–3736.
- [29] R. Crompton, H. Williams, D. Ansell, L. Campbell, K. Holden, S. Cruickshank, M. J. Hardman, *Lab. Invest.* **2016**, *96*, 439–449.
- [30] G. Celenza, C. Luzi, M. Aschi, B. Segatore, D. Setacci, C. Pellegrini, C. Forcella, G. Amicosante, M. Perilli, *J. Antimicrob. Chemother.* **2008**, *62*, 991–997.
- [31] R. A. Copeland, *Enzyme: A Practical Introduction to Structure, Mechanism and Data Analysis*, Wiley, New York, **2000**.
- [32] W. X. Tian, C. L. Tsou, *Biochemistry* **1982**, *21*, 1028–1032.
- [33] T. Mosmann, *Journal of Immunological Methods.* **1983**, *65* (1–2): 55–63.
- [34] N. C. J. Strynadka, M. Eisenstein, E. Katchalski-Katzir, B. K. Shoichet, I. D. Kuntz, R. Abagyan, M. Totrov, J. Janin, J. Cherfils, F. Zimmerman, et al., *Nat Struct Mol Biol* **1996**, *3*, 233–239.
- [35] A. C. Wallace, R. A. Laskowski, J. M. Thornton, *Protein Eng.* **1995**, *8*, 127–134.
- [36] E. Krissinel, *J. Mol. Biochem.* **2012**, *1*, 76–85.
- [37] D. C. Marciano, N. G. Brown, T. Palzkill, *Protein Sci.* **2009**, *18*, 2080–2089.
- [38] N. C. Strynadka, H. Adachi, S. E. Jensen, K. Johns, A. Sielecki, C. Betzel, K. Sutoh, M. N. James, *Nature* **1992**, *359*, 700–705.
- [39] P. Bellio, B. Segatore, A. Mancini, L. Di Pietro, C. Bottoni, A. Sabatini, F. Brisdelli, M. Piovano, M. Nicoletti, G. Amicosante, et al., *Phytomedicine* **2015**, *22*, 223–230.
- [40] W. R. Greco, G. Bravo, J. C. Parsons, *Pharmacol. Rev.* **1995**, *47*, 331–385.
- [41] F. C. Odds, *J. Antimicrob. Chemother.* **2003**, *52*, 1.
- [42] S. Monaco, E. Gordon, M. W. Bowler, S. Delageniere, M. Guijarro, D. Spruce, O. Svensson, S. M. McSweeney, A. A. McCarthy, G. Leonard, et al., *J. Appl. Crystallogr.* **2013**, *46*, 804–810.
- [43] P. R. Evans, G. N. Murshudov, *Acta Crystallogr. D. Biol. Crystallogr.* **2013**, *69*, 1204–1214.
- [44] A. J. McCoy, R. W. Grosse-Kunstleve, P. D. Adams, M. D. Winn, L. C. Storoni, R. J. Read, *J. Appl. Crystallogr.* **2007**, *40*, 658–674.
- [45] G. N. Murshudov, P. Skubák, A. A. Lebedev, N. S. Pannu, R. A. Steiner, R. A. Nicholls, M. D. Winn, F. Long, A. A. Vagin, *Acta Crystallogr. Sect. D* **2011**, *67*, 355–367.
- [46] P. Emsley, B. Lohkamp, W. G. Scott, K. Cowtan, *Acta Crystallogr. Sect. D* **2010**, *66*, 486–501.
- [47] N. W. Moriarty, R. W. Grosse-Kunstleve, P. D. Adams, *Acta Crystallogr. D. Biol. Crystallogr.* **2009**, *65*, 1074–1080.
- [48] P. V. Afonine, R. W. Grosse-Kunstleve, N. Echols, J. J. Headd, N. W. Moriarty, M. Mustyakimov, T. C. Terwilliger, A. Urzhumtsev, P. H. Zwart, P. D. Adams, *Acta Crystallogr. D. Biol. Crystallogr.* **2012**, *68*, 352–367.

## Entry for the Table of Contents



This study focuses on the design of new phenyl boronic acid derivatives active vs KPC-2 carbapenemase with nanomolar affinity. New derivatives were able to restore susceptibility to meropenem in clinical strains overexpressing KPC-2 and resulted not cytotoxic against human cells. The crystallographic binary complexes of best inhibitors binding KPC-2 were obtained at high resolution. Kinetic descriptions of slow binding, time dependent inhibition and interactions geometries in KPC-2 were fully investigated.